Int. J. Heat Mass Transfer. Vol. 31, No. 4, pp. 673–693, 1988
Printed in Great Britain

0017–9310/88 $3.00+0.00

Natural convection in open-ended cavities with a porous obstructing medium

J. ETTEFAGH and K. VAFAI
Department of Mechanical Engineering, 206 West 18th Avenue, Columbus, OH 43210, U.S.A.

(*Received* 21 *January* 1987 *and in final form* 10 *July* 1987)

Abstract—The buoyancy-driven convection in an open-ended cavity with an obstructing medium such as a porous material is analyzed in this work. The numerical results of the flow and temperature fields for the range of Darcy–Rayleigh number, $Ra \leqslant 350$ are given. The importance of the external corners in vorticity generation and flow instability augmentation is discussed. The presence of 'humps' as well as the periodic behavior in the variation of the Nusselt number with time are studied. The effects of important variables such as the aspect ratio, the temperature difference, and the Darcy–Rayleigh number on the flow field and the cavity Nusselt number are investigated. Comparisons are also made with previously reported studies of natural convection in a cavity filled with a porous medium.

1. INTRODUCTION

BUOYANCY-driven natural convection is an important mode of heat transfer in many engineering systems. Among various problems in natural convection, internal flows within enclosures have been studied extensively due to its widespread engineering applications [1–6]. Numerous analytical, numerical and experimental results are readily available for enclosures with rectangular boundaries. The influence of important parameters such as the Darcy–Rayleigh number and the cavity aspect ratio has been thoroughly investigated for these enclosures. However, relatively few studies have been directed to thermally induced motion in open cavities or partial enclosures. The engineering applications of open cavities are important; for example, fire spread in rooms, solar thermal central receiver systems, connections between reservoirs, nuclear waste repository, and the brake housing commonly employed in a number of aircraft models. In recent years the buoyancy-driven convection in open cavities with a regular medium such as air has received some attention [7–9], but the flow and heat transfer processes in open as well as open-ended cavities with a porous obstructing medium remain to be investigated. This paper concentrates on the later case which is more general and complicated. The results for the open cavity case can be deduced from the open-ended cavity problem.

The importance of flow and heat transfer in open-ended cavities is further enhanced due to its basic geometry. This is because a number of complex geometries can be constructed from this basic geometry. An important consideration in an open-ended cavity problem is the treatment of the boundary conditions. In this study the open boundary conditions were taken into account accurately and with relative ease in the numerical scheme.

In the present work the buoyancy-driven flow and heat transfer in an open-ended cavity are modeled as a transient two-dimensional problem. The effects of important variables such as the aspect ratio, the different temperature levels, and the Darcy–Rayleigh number on the flow field and the Nusselt number are investigated. The results are presented in terms of the streamlines and the temperature contour plots.

The results show some interesting interaction between the flow and temperature fields in an open-ended cavity. The results also indicate that the flow field inside an open-ended cavity and in the vicinity of the aperture planes is relatively insensitive to the boundary conditions provided that the computational domain is extended far enough from the openings. The results also illustrate the dependence of thermal losses on temperature levels as well as the existence of time-dependent variations in flow and in the Nusselt number. The presence of 'humps' in the variations of the Nusselt number with time is investigated. Furthermore, the periodic behavior of the Nusselt number as a result of the recirculating eddies next to the lower block is illustrated and discussed. The results show the influence of the external corners in an open-ended cavity which augments the flow instabilities. The result also indicates that decreasing the aspect ratio has a stabilizing effect on the flow field.

2. MATHEMATICAL FORMULATION

The present study considers an incompressible, transient, two-dimensional thermally driven buoyant natural convection flow due to the temperature differential in an open-ended cavity as shown in Fig. 1. The geometry corresponds to a two-dimensional slot which is exposed to an ambient temperature T_∞. The lower and upper temperatures of the slot are T_1 and T_2, respectively. The vertical portions of the two blocks are assumed to be adiabatic. The governing equations for flow through homogeneous porous

NOMENCLATURE

A	aspect ratio, h/d
d	horizontal extent of the open-ended cavity [m]
g	gravitational acceleration [m s^{-2}]
h	vertical extent of the open-ended cavity [m]
Nu	Nusselt number
Ra	Darcy–Rayleigh number, $\kappa g\beta h\Delta T/\nu\alpha_e$
t	time [s]
T	temperature [K]
T_1	lower block temperature [K]
T_2	upper block temperature [K]
T_∞	free-stream temperature [K]
u	x-component velocity [m s^{-1}]
v	y-component velocity [m s^{-1}]
x	spatial coordinate, horizontal [m]
X	dimensionless spatial coordinate, horizontal, x/d
y	spatial coordinate, vertical [m]
Y	dimensionless spatial coordinate, vertical, y/d.

Greek symbols

α_e	effective thermal diffusivity [m^2 s^{-1}]
β	coefficient of volume expansion [K^{-1}]
ε	accuracy of calculation
θ	dimensionless temperature, $(T-T_\infty)/(T_1-T_\infty)$
κ	permeability
ν	kinematic viscosity [m^2 s^{-1}]
ξ	dimensionless vorticity
σ	thermal capacitance
τ	dimensionless time, $\alpha_e t/\sigma d^2$
ϕ	general dimensionless field variable
ψ	dimensionless streamfunction.

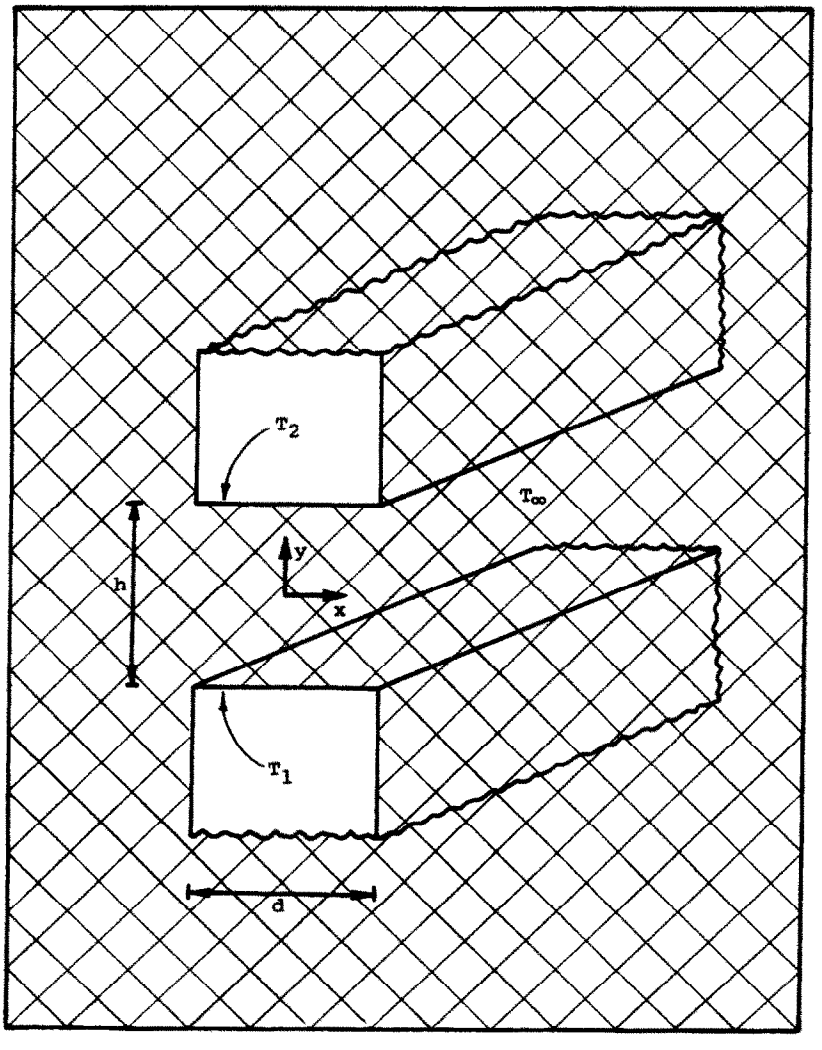

FIG. 1. Schematic of an open-ended cavity with an obstructing porous medium.

media with Boussinesq approximation are

$$\frac{\partial u}{\partial y}-\frac{\partial v}{\partial x}=-\frac{\kappa g\beta}{\nu}\frac{\partial T}{\partial x} \tag{1}$$

$$\sigma\frac{\partial T}{\partial t}+u\frac{\partial T}{\partial x}+v\frac{\partial T}{\partial y}=\alpha_e\left(\frac{\partial^2 T}{\partial x^2}+\frac{\partial^2 T}{\partial y^2}\right). \tag{2}$$

This formulation is based on the following assumptions: (a) small temperature difference; (b) constant fluid properties except for the temperature effect in density variation; (c) an incompressible fluid; and (d) neglect of viscous heat dissipation. It should be noted that Darcy's law is used to represent the flow field which neglects the boundary and inertial effects. These effects can become important for convective type flows [10], however, they are neglected in this study. Equations (1) and (2) may be made dimensionless by introducing

$$X=\frac{x}{d}, \qquad Y=\frac{y}{d}$$

$$u=\frac{\alpha_e}{d}\frac{\partial\psi}{\partial Y}, \qquad v=-\frac{\alpha_e}{d}\frac{\partial\psi}{\partial X}$$

$$\theta=\frac{T-T_\infty}{T_1-T_\infty}, \qquad \tau=\frac{\alpha_e}{\sigma d^2}t$$

$$Ra=\frac{\kappa g\beta h\Delta T}{\alpha_e\nu}, \qquad \Delta T=T_1-T_\infty.$$

The resultant field equations in terms of the stream-function and the vorticity are

$$\xi=-Ra\frac{\partial\theta}{\partial X} \tag{3}$$

$$\nabla^2\psi=\xi \tag{4}$$

$$\frac{\partial\theta}{\partial\tau}+\frac{\partial\psi}{\partial Y}\frac{\partial\theta}{\partial X}-\frac{\partial\psi}{\partial X}\frac{\partial\theta}{\partial Y}=\nabla^2\theta. \tag{5}$$

The corresponding boundary conditions for an open-ended cavity as shown in Fig. 2 are

$$\psi=0,\theta=1 \quad \text{at} \quad Y=-\frac{A}{2} \quad \text{for} \quad -\tfrac{1}{2}\leqslant X\leqslant\tfrac{1}{2} \tag{6}$$

$$\psi=0,\theta=\theta_2 \quad \text{at} \quad Y=\frac{A}{2} \quad \text{for} \quad -\tfrac{1}{2}\leqslant X\leqslant\tfrac{1}{2} \tag{7}$$

$$\psi=0,\frac{\partial\theta}{\partial X}=0 \quad \text{at} \quad X=\pm\tfrac{1}{2} \quad \text{as} \quad Y\to\pm\infty \tag{8}$$

$$V=0,\frac{\partial\theta}{\partial X}=0 \quad \text{as} \quad X\to\pm\infty, \quad \text{for all} \quad Y \tag{9}$$

$$\frac{\partial U}{\partial Y}=0,\frac{\partial\theta}{\partial Y}=0 \quad \text{as} \quad Y\to\pm\infty, \quad \text{for all} \quad X. \tag{10}$$

It should be noted that a number of numerical runs were made with several different far field boundary conditions. Among which equations (9) and (10) were chosen since they provided consistent numerical results.

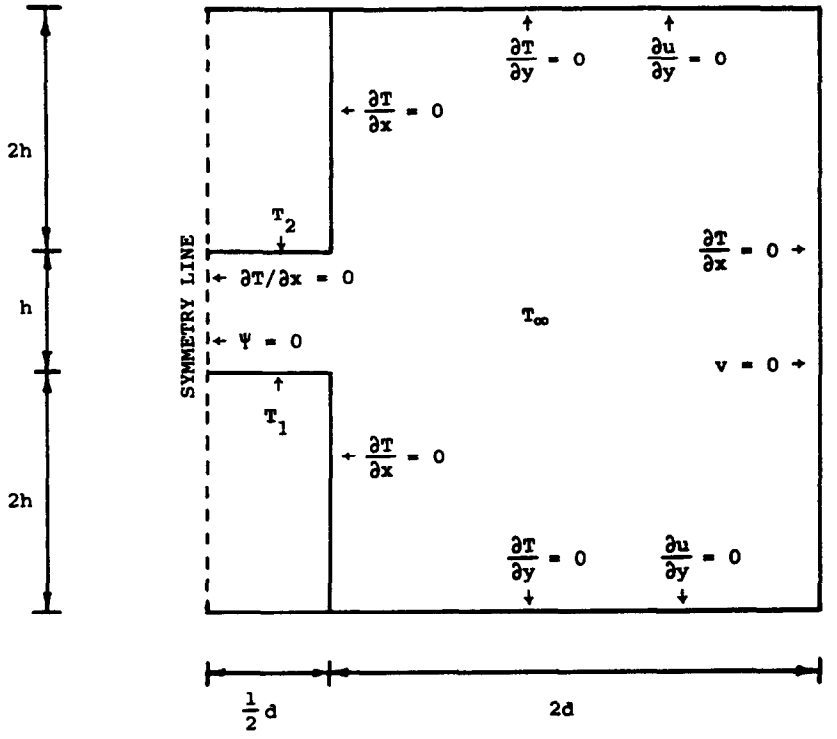

FIG. 2. Schematic of the geometry of the problem with symmetry consideration and the boundary conditions used.

Due to symmetry of the problem, the corresponding boundary conditions at the line of symmetry are

$$\psi = 0, \frac{\partial \theta}{\partial X} = 0 \quad \text{at} \quad X = 0, \quad \text{for} \quad -\frac{A}{2} \leqslant Y \leqslant \frac{A}{2}. \tag{11}$$

The symmetry conditions were checked by performing a number of numerical runs for the entire open-ended cavity without using the symmetry conditions. It was found that the symmetry conditions do indeed exist. A preliminary experimental investigation based on the open-ended cavity geometry also confirmed the symmetry conditions. As a consequence of the symmetry consideration the geometry of the problem is translated to that of an open cavity, i.e. a cavity of rectangular cross-section with one side face removed, as shown in Fig. 2. Therefore, the results presented here are also valid for the natural convection in open cavities with a porous obstructing medium subjected to the above boundary conditions. The initial conditions are

$$\psi = \xi = \theta = 0 \quad \text{everywhere at} \quad \tau = 0 \tag{12a}$$

except for

$$\theta = 1 \quad \text{at} \quad Y = -\frac{A}{2}, \quad \text{for} \quad -\tfrac{1}{2} \leqslant X \leqslant \tfrac{1}{2} \tag{12b}$$

$$\theta = \theta_2 \quad \text{at} \quad Y = -\frac{A}{2}, \quad \text{for} \quad \tfrac{1}{2} \leqslant X \leqslant \tfrac{1}{2}. \tag{12c}$$

The analysis of natural convection in an open-ended cavity with porous obstructing medium will encompass the simultaneous solution of governing equations (3)–(5) subject to the boundary and initial conditions given by equations (6)–(12).

Introducing an overall cavity Nusselt number as the sum of the lower and upper blocks Nusselt numbers and employing the dimensionless variables yields

$$Nu = -\int_0^1 \left.\frac{\partial \theta}{\partial Y}\right|_{Y=-A/2} \mathrm{d}X + \frac{1}{\theta_2}\int_0^1 \left.\frac{\partial \theta}{\partial Y}\right|_{Y=A/2} \mathrm{d}X. \tag{13}$$

The rate of heat transfer from the lower and upper blocks to the fluid inside the open-ended cavity requires the solution of equation (13).

3. NUMERICAL SOLUTION

In most natural convection flows of practical interest, a complete analytical solution is not possible and one has to depend on the numerical technique to obtain the desired results. The governing equations (3)–(5) form a coupled non-linear partial differential equation that must be solved subject to the boundary conditions given by equations (6)–(10). The numerical scheme is based on finite difference versions of the governing equations. The time-dependent energy equation (5) was solved by ADI, a two-step implicit method. This method leads to a tridiagonal matrix of unknown temperatures which is then inverted by the Thomas algorithm. It should be noted that at any node, the velocities are evaluated at time n and are treated as constant over that time step. The numerical solution to the streamfunction equation (4) was obtained by SOR, an implicit iteration method. The over-relaxation parameter of 1.75 was found to cause the optimum convergence rate. The convergence criterion for steady state solution was met when the relative difference in two consecutive time steps satisfied a prescribed tolerance given by

$$\frac{\phi_{i,j}^{n+1} - \phi_{i,j}^{n}}{\phi_{i,j}^{n+1}} \leqslant \varepsilon$$

where $\phi_{i,j}$ is a general symbol used for ψ, ξ, and θ. The tolerance ε was set to 10^{-3} for all three variables. It should be noted that at higher Darcy–Rayleigh numbers convergence was significantly faster for both temperature and streamfunction than the vorticity.

To increase the accuracy and stability of the numerical scheme, the derivatives at the boundaries were incorporated through the governing equations. The vorticity boundary conditions were calculated directly from the vorticity transport equation (3) which is more consistent with the assumptions that are inherent in Darcy's law. Since there are two kinds of temperature boundary conditions imposed on the convex corners, the numerical temperature evaluation of these points requires special consideration. For this reason at convex corners a multi-valued procedure [11, 12] for the temperature calculations was used. This method assumes a different temperature value at the corner point for each directional derivative. In order to simulate the open-ended region, the computational domain was systematically extended in both the horizontal and vertical direction. It was found that the reduction of the numerical domain to twice the length of the slot ($2d$) in the $\pm x$-direction and twice the height of the opening ($2h$) in the $\pm y$-direction was sufficient enough to simulate the open boundaries without any significant changes of the flow field inside the open-ended cavity. It should be noted that the effects of open boundaries and their extensions should be further studied.

4. RESULTS AND DISCUSSION

Calculations were performed for values of $Ra \leqslant 350$. The bulk of the numerical runs were performed for an aspect ratio of $\frac{1}{2}$ (which translates to an open cavity of square cross-section), a lower block temperature of $\theta_1 = 1$, and an upper block temperature of $\theta_2 = 1$. In order to study the effects of aspect ratio, numerical solutions for aspect ratios of 1 and $\frac{1}{4}$ were obtained. Furthermore, the effects of the relative temperature variations between the lower and upper blocks were investigated. In all cases the full transient behavior of the cavity Nusselt number were studied. In the remainder of this work, the term 'open

cavity', which corresponds to the geometry of half of an open-ended cavity, will be used for convenience.

The present results were obtained on an equally spaced grid of 51×51 points with 121 points inside the open cavity for an aspect ratio of $\frac{1}{2}$. The total number of grid points varied for the cases with different aspect ratios, but in all cases, at least 121 points were used inside the open cavity. The typical time increment used was 3×10^{-3}. Due to the uniform grid spacing employed in this work and the extensions of the open boundaries, increasing the number of grid points inside the open cavity would result a large increase in computational time. Although for low Rayleigh flows the results are fairly accurate, the

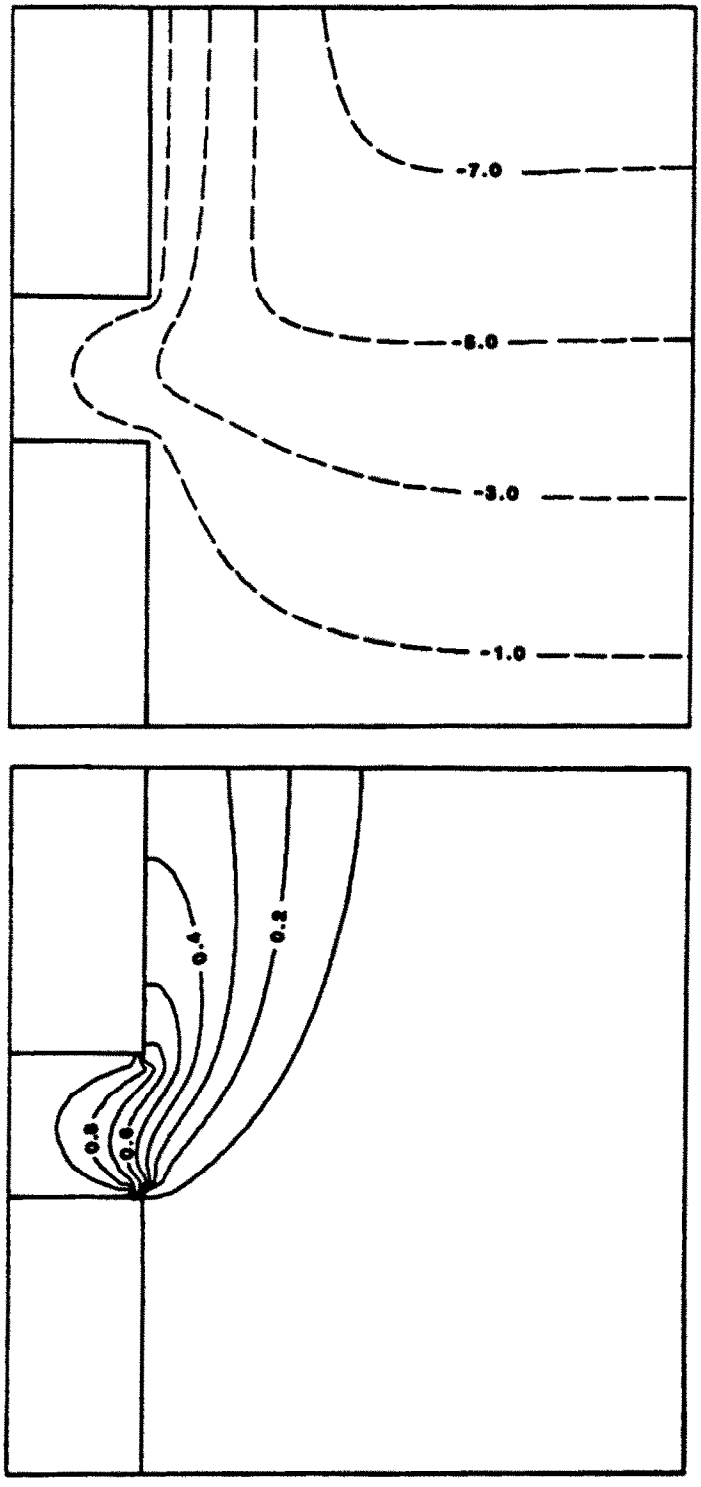

FIG. 3. Streamlines and isotherms for $\theta_2 = 1$, $A = \frac{1}{2}$ and $Ra = 20$ at steady state.

results for higher Rayleigh flows $Re > 250$ do give a good qualitative representation of the results. For more accurate results we need to employ the variable grid spacing. In fact, based on some preliminary runs with variable grids, we know that the given results especially for lower Rayleigh flows are fairly accurate.

As shown in Fig. 3 for $Ra = 20$, the heat transfer mechanism inside the open cavity is conduction dominated. However, the convection mode of heat transfer is not totally insignificant, as indicated by the distortion of the temperature field in Fig. 3. This distortion lowers the conduction heat transfer in the vicinity of the aperture plane, where the convection contribution is responsible for most of the heat transfer. The flow field inside the open cavity is almost symmetric about the mid-height plane. Since the streamlines cannot cross over, the symmetry line serves to turn the flow 180°. The hot fluid exiting the open cavity will rise due to buoyancy and is faster than the flow inside the open cavity. The cold incoming fluid is sucked inside the open cavity from the lower part of the aperture at an angle. This is primarily because of the replacement of hot fluid exiting from the upper part of the open cavity. This suction mechanism is responsible for an almost parallel flow along the lower block due to the replacement of fluid rising up along the symmetry line. At the same time as this flow travels along the lower block, the fluid is also heated from below due to the higher temperature of the lower block. As a result, there exists a conflict between the buoyancy forces and horizontal driving forces acting on the fluid particles with respect to time. These conflicting driving mechanisms are expected to cause 'humps' in the transient variations of the cavity Nusselt number. This effect is indeed observed, as it is discussed in more detail later on.

As Ra increases (20–100), the cold fluid penetrates further inside the open cavity. The streamlines and isotherms are spaced closer together in the vicinity of the lower block, as shown in Fig. 4. As a result of larger temperature gradient, the heat transfer from the lower block increases. The heat transfer from the upper block, which is mainly by conduction, also increases. The outgoing flows are much faster than the incoming flows. As a result, the flow field is no longer symmetric since the incoming flows occupy a larger portion of the open cavity. The approaching flow from the far field is either sucked into the open cavity or is carried up due to the viscous effect. As the Darcy–Rayleigh number increases, the horizontal temperature gradient for the outgoing flows close to the upper block decreases. As shown in Fig. 4 for $Ra = 100$, the isotherm near the upper block is almost horizontal and the thermally-stratified flow occurs along the upper block. The outgoing streamlines are also spaced closer together along the vertical insulated wall. This indicates the early stage of the wall plume formation. The interaction of the wall with the plume is to attract the plume toward it, as shown in Fig. 4.

As Ra increases from 100 to 350, the incoming cold fluid penetrates much further inside the open cavity. Comparison of Figs. 4 and 5 shows that the streamlines and isotherms near the lower block are more clustered together for higher Ra. It also indicates that, as Ra increases, the incoming flow enters the open cavity at much faster rates. As a result of these higher velocities, the thermal boundary layer development along the lower block, which was witnessed for the case of $Ra = 100$, becomes thinner, as shown in Fig. 5. As it can be seen from Figs. 5 to 7, as Ra increases, the number of horizontal isotherms close to the upper block increases, resulting in a thicker region of the thermally-stratified flow in the upper part of the open cavity. The outgoing hot fluid also exits the aperture and rises up at much faster velocities, leading to a thinner wall plume along the upper insulated vertical boundary.

As discussed earlier, there are two conflicting driving mechanisms, i.e. horizontal driving forces and buoyancy forces, acting on the fluid particles along the lower block. For larger Ra, the buoyancy forces become more important and are responsible for the shape of isotherms close to the lower block, as shown in Figs. 6 and 7. This effect eventually leads to thermal instabilities for $Ra = 350$, where it was not possible to reach the steady state solution. Figure 7 shows the formation of a vortex in the central region of the open cavity. This is due to the viscous effect associated with the high velocities of the incoming and outgoing fluids. This vortex formation causes the incipience of the temperature distribution instabilities in the vicinity of the lower corner.

Figures 8 and 9 illustrate the time evolution of the flow and temperature fields for $Ra = 200$ at consecutive times within a cycle of $3\Delta\tau$ apart. The effect of the external corners in vorticity generation is clearly depicted in Fig. 8. As the time progresses, the central vortex moves out of the upper part of the aperture plane. The shapes of isotherms along the three boundaries of the open cavity in Fig. 8 clearly show the presence of thermal instabilities inside the open cavity. These thermal instabilities may be explained by the two conflicting driving mechanisms acting on the fluid particles traveling along the lower block of the open cavity, as discussed earlier, i.e. horizontal driving forces and buoyancy forces. As a result, there exist small recirculating flow regions, or eddies, which are convected along the lower block and vertically upward along the symmetry line. Figure 9 indicates that, as the circulating flows move out of the top boundary of the computational domain, their viscous effects tend to smear out, giving rise to a parallel flow coming from the right boundary. The presence of the parallel flow clearly verifies the existence of rotational flow away from the openings and the accuracy of the far field boundary conditions used.

In order to study the effects of different temperature levels on the flow and temperature fields, numerical runs were performed with upper block temperatures

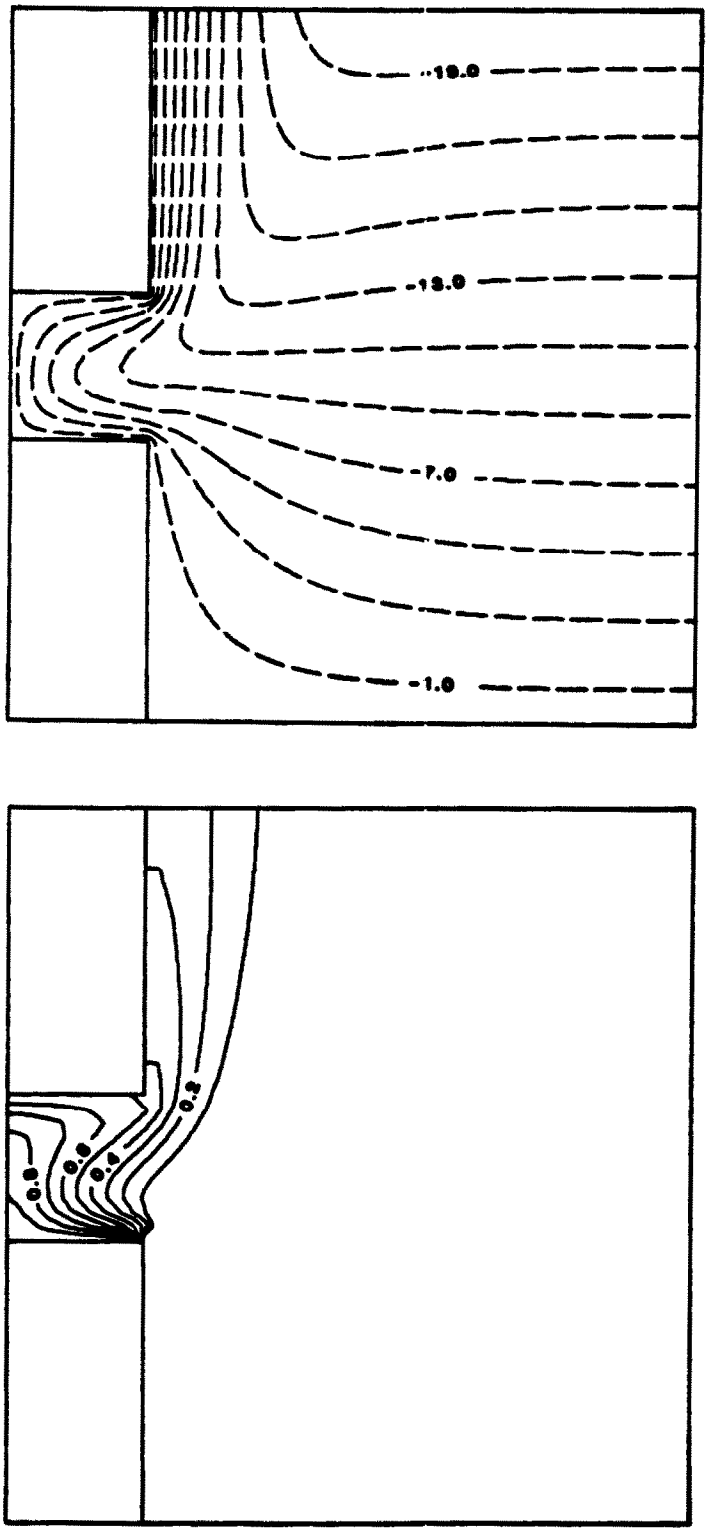

FIG. 4. Streamlines and isotherms for $\theta_2 = 1$, $A = \frac{1}{2}$ and $Ra = 100$ at steady state.

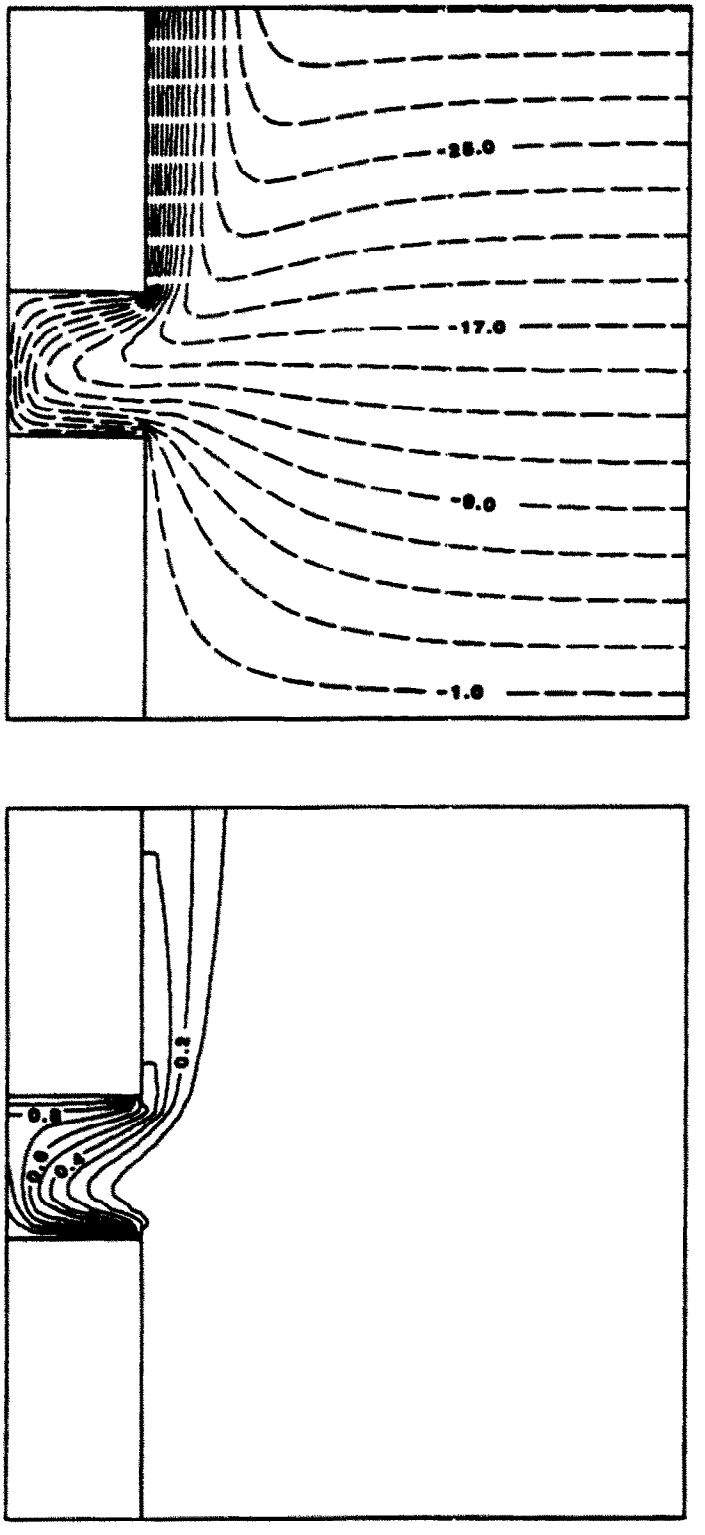

FIG. 5. Streamlines and isotherms for $\theta_2 = 1$, $A = \frac{1}{2}$ and $Ra = 200$ at steady state.

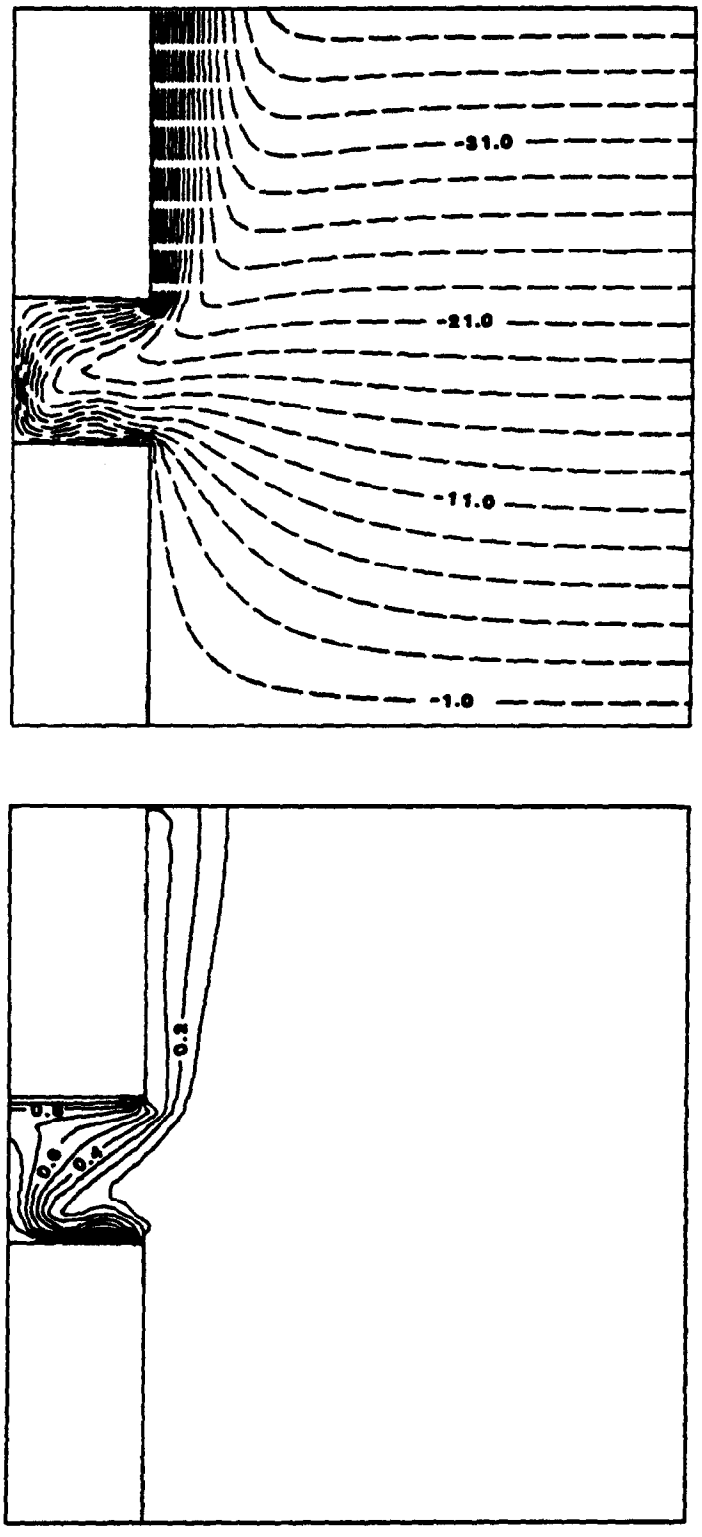

FIG. 6. Streamlines and isotherms for $\theta_2 = 1$, $A = \frac{1}{2}$ and $Ra = 250$ at steady state.

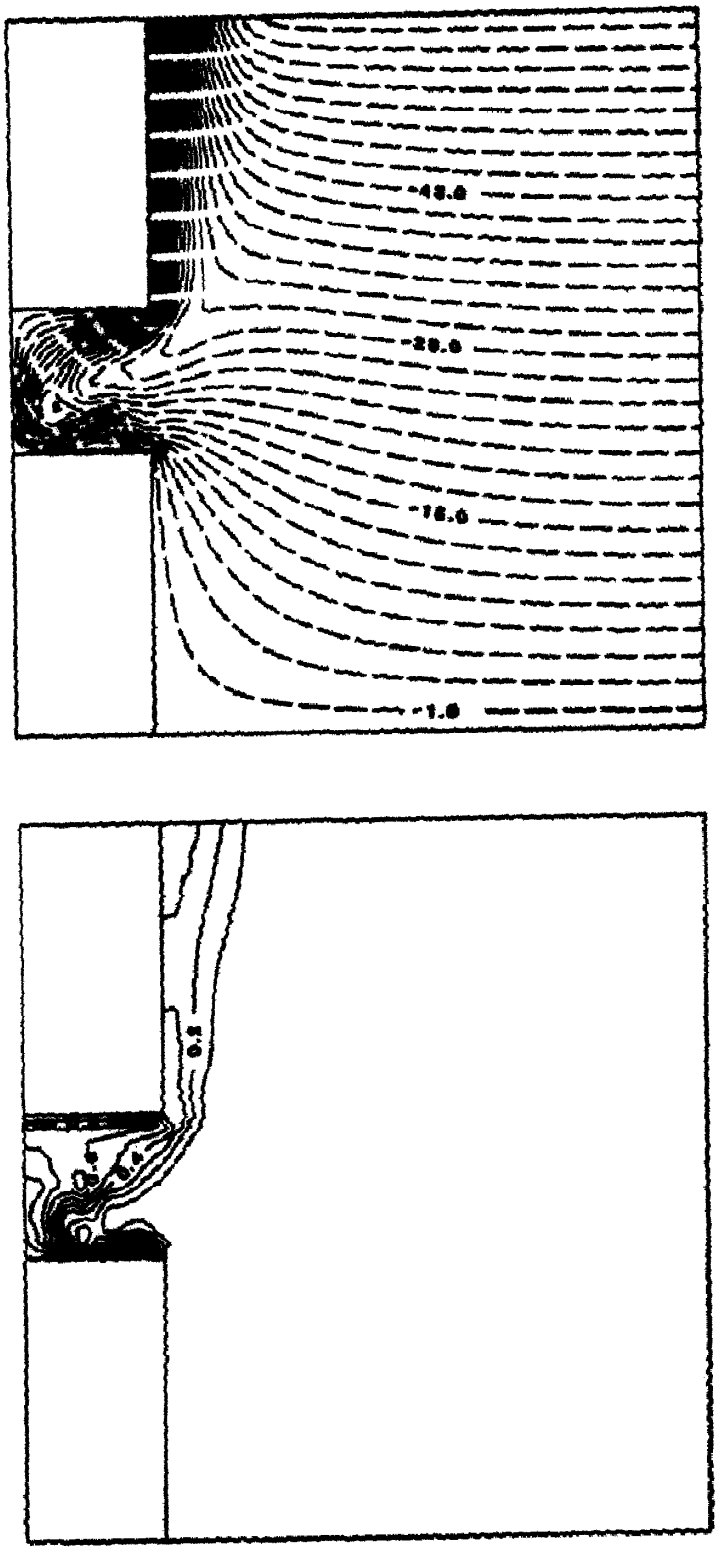

FIG. 7. Streamlines and isotherms for $\theta_2 = 1$, $A = \frac{1}{2}$ and $Ra = 350$ at steady state.

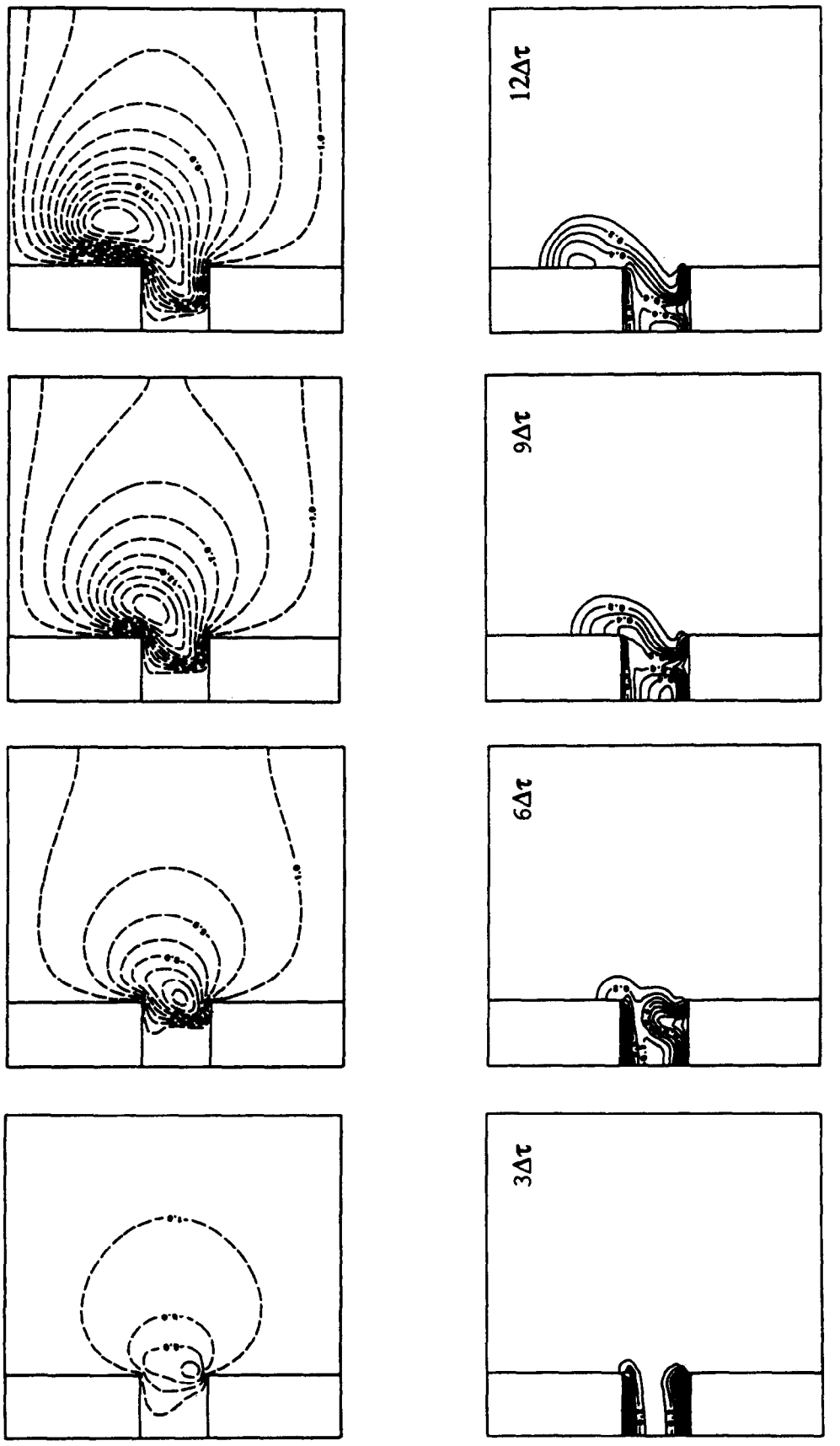

FIG. 8. Streamlines and isotherms for $\theta_2 = 1$, $A = \frac{1}{2}$ and $Ra = 200$ at $3\Delta\tau \leqslant \tau \leqslant 12\Delta\tau$.

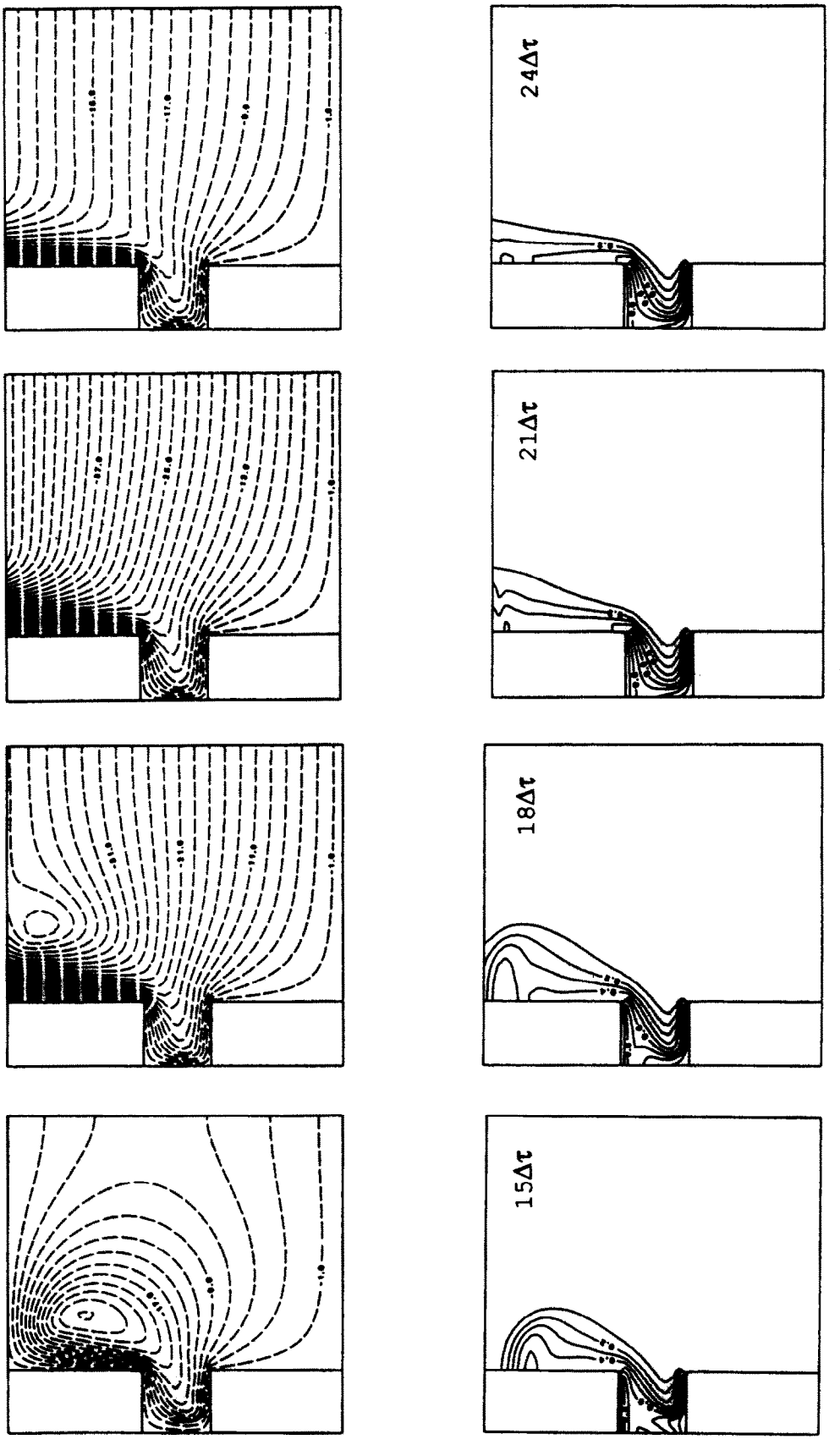

FIG. 9. Streamlines and isotherms for $\theta_2 = 1$, $A = \frac{1}{2}$ and $Ra = 200$ at $15\Delta\tau \leqslant \tau \leqslant 24\Delta\tau$.

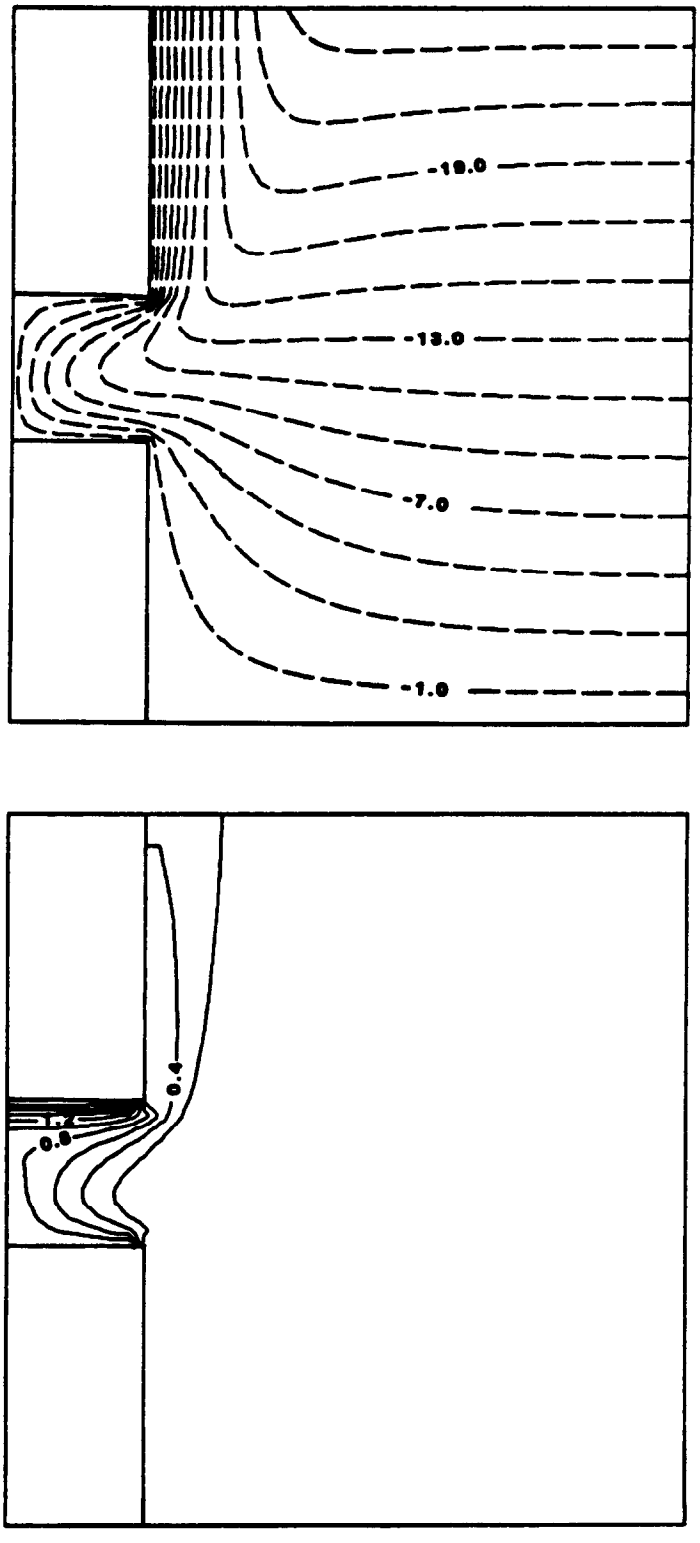

FIG. 10. Streamlines and isotherms for $\theta_2 = 2$, $A = \frac{1}{2}$ and $Ra = 100$ at steady state.

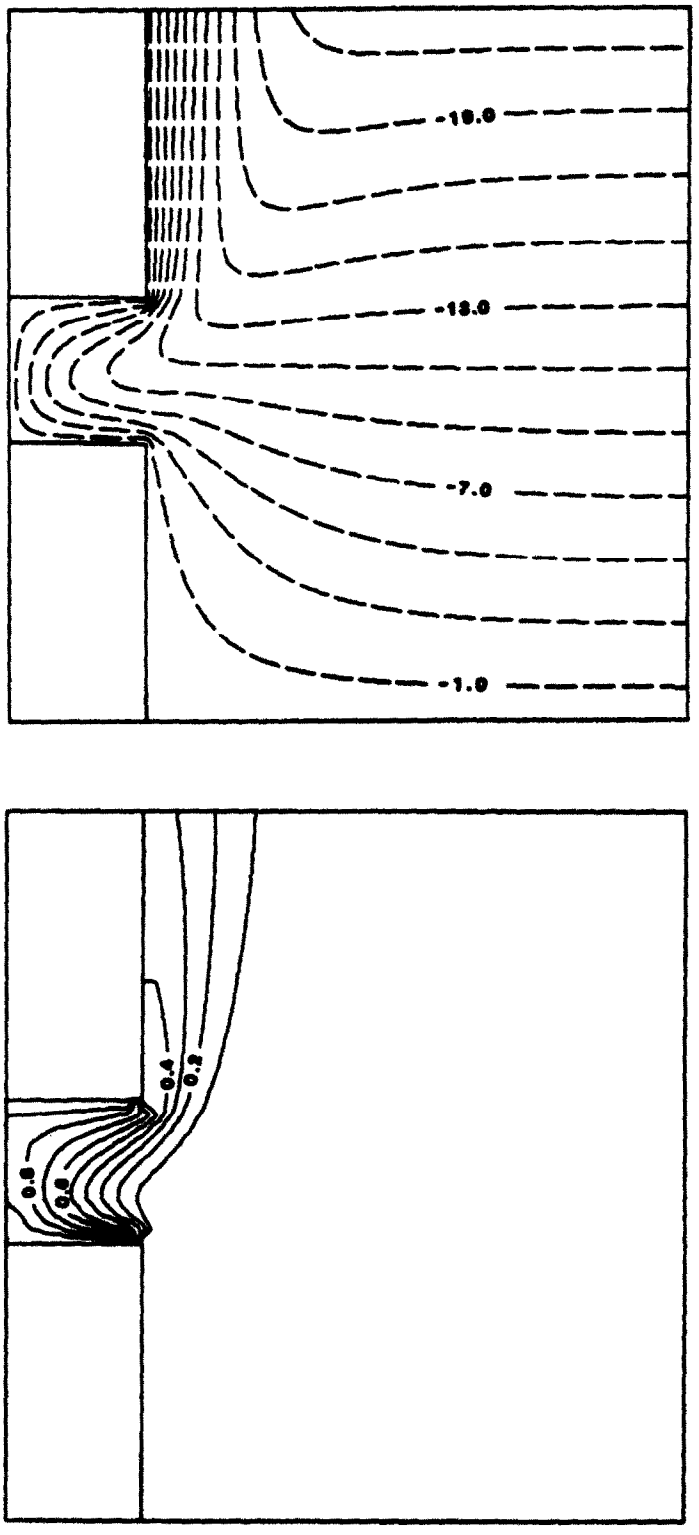

FIG. 11. Streamlines and isotherms for $\theta_2 = \frac{1}{2}$, $A = \frac{1}{2}$ and $Ra = 100$ at steady state.

of $\theta_2 = 2$ and $\frac{1}{2}$. The results were obtained for an aspect ratio of $\frac{1}{2}$ and lower block temperature of $\theta_1 = 1$, and the Darcy–Rayleigh number of $Ra = 100$. These results are presented in Figs. 10 and 11, respectively.

As the upper block temperature increases ($\theta_2 = 2$), the general observations made for the case of $\theta_2 = 1$ are also valid for this case with few remarks. Comparison of Fig. 10 with its corresponding case of $\theta_2 = 1$, shown in Fig. 4 indicates that, as θ_2 increases, the thermally-stratified flow region in the upper part of the open cavity is much thicker and forms at lower Darcy–Rayleigh number. Consequently, due to higher buoyancy forces associated with the outgoing flows, they rise up with higher velocities, resulting in a thinner wall plume.

As the upper block temperature decreases ($\theta_2 = \frac{1}{2}$), most of the general observations made for the case of $\theta_2 = 1$ are also valid for this case with few exceptions. The major difference lies in the rate of heat transfer from the upper block to the fluid particles inside the open cavity. In general, the major heat transfer contribution due to the temperature difference between the upper block and that of the environment is by conduction. However, for the case of $\theta_2 = \frac{1}{2}$, the conduction effect is only limited to the early parts of the flow development when the initially cold fluid particles have not yet assumed high enough temperature levels. Once the fluid inside the open cavity reaches the temperature levels above that of the upper block, then the direction of heat transfer is reversed and heat would be transferred from the fluid to the isothermal upper block. But, for the case of $\theta_2 = 1$, the direction of the heat transfer from the upper block to the fluid remains unchanged. This is basically due to the fact that the temperature of fluid particles everywhere inside the open cavity is less than the upper block temperature. Consequently, as it can be seen from Fig. 11, the formation of the thermally-stratified flow region along the upper block does not occur for the case of $\theta_2 = \frac{1}{2}$.

Numerical runs with aspect ratios of 1 and $\frac{1}{4}$ were performed to investigate the effects of aspect ratio on the flow and temperature fields. The solutions were obtained for a fixed Darcy–Rayleigh number of $Ra = 100$, lower block temperature of $\theta_1 = 1$, and upper block temperature of $\theta_2 = 1$. The corresponding streamlines and isotherms are presented in Figs. 12 and 13. Comparison of these results with the corresponding case of $A = \frac{1}{2}$ (Fig. 4) indicates that, as the aspect ratio increases, the incoming cold fluid penetrates further inside the open cavity. As a result, the fluid flow instabilities are expected to occur earlier. This fact has been indeed confirmed by the numerical results. The above comparison also indicates that, as the aspect ratio increases from $\frac{1}{2}$ to 1, the thickness of the thermally-stratified flow region increases while, for the case of $A = \frac{1}{4}$, the thermal stratification does not occur. It should be noted that, for the case of $A = \frac{1}{4}$, a stagnant fluid region exists where the heat transfer mechanism is conduction dominated. An increase in aspect ratio also has an effect on amplifying the unsteady behavior of the heat transfer from the lower block.

4.1. *Heat transfer results*

The cavity Nusselt number calculations were performed by numerically integrating expression (13) using Simpson's rule. The transient behavior of the Nusselt number for $\theta_2 = 1$, $A = \frac{1}{2}$ and different Darcy–Rayleigh numbers are shown in Fig. 14.

Initially, the sharp gradients near the lower and upper blocks are responsible for a rapid rate of heat transfer and their corresponding high Nusselt numbers. As shown in Fig. 14(a), for $Ra \leqslant 200$, the cavity Nusselt number oscillates with a decaying amplitude. These oscillations are due to the existence of thermal instabilities in the early stages of the flow development, as previously discussed. As time increases, the cavity Nusselt number asymptotically approaches a steady state value. Figure 14(a) shows that an increase in Ra will result in earlier presence of 'humps'. This is expected since the time for the heating process of the fluid particles along the lower block to take place decreases for the higher Ra flows. For higher Darcy–Rayleigh numbers, as these 'heat bubbles' move, diffusion effects have less chance to smear out their thermal identities. Consequently, as Ra increases, the frequency of the oscillations in the cavity Nusselt number increases. For values of $Ra \geqslant 250$, the unsteadiness appears as a sequence of recirculating eddies, or 'hot spots', with respect to time. As a result, the Nusselt number exhibits a periodic behavior with respect to time, as illustrated in Fig. 14(a). It should be noted that this type of quasi steady fluctuations of the Nusselt number is characteristic of an open cavity system with a porous obstructing medium and does not appear to occur in a closed cavity system.

Figures 14(b) and (c) present the typical transient behavior of the upper block, lower block and cavity Nusselt numbers for $Ra = 200$ and 350, respectively. As it can be seen from the above figures, the bottom block Nusselt number, Nu_B, is higher than the one for the top block, Nu_T. This is primarily due to the fact that the heat transfer from the upper block is mainly by conduction, whereas the heat transfer from the lower block is convection dominated. As discussed earlier, due to thermal instabilities along both blocks, the corresponding Nusselt numbers would exhibit an oscillatory behavior, which are shown in Fig. 14(b). Figure 14(c) shows that the periodic behavior of both the upper and lower block Nusselt numbers have the same period, which leads to an overall periodic behavior of the cavity Nusselt number having an amplitude equal to the sum of each individual amplitude. Figure 14(c) also shows that the amplitude of the upper block Nusselt number is greater than the corresponding one for the lower block. This effect is explained by the fact that the flow along the upper block starts out with an inherent instability passed on from the flow situation over the lower block. Figure

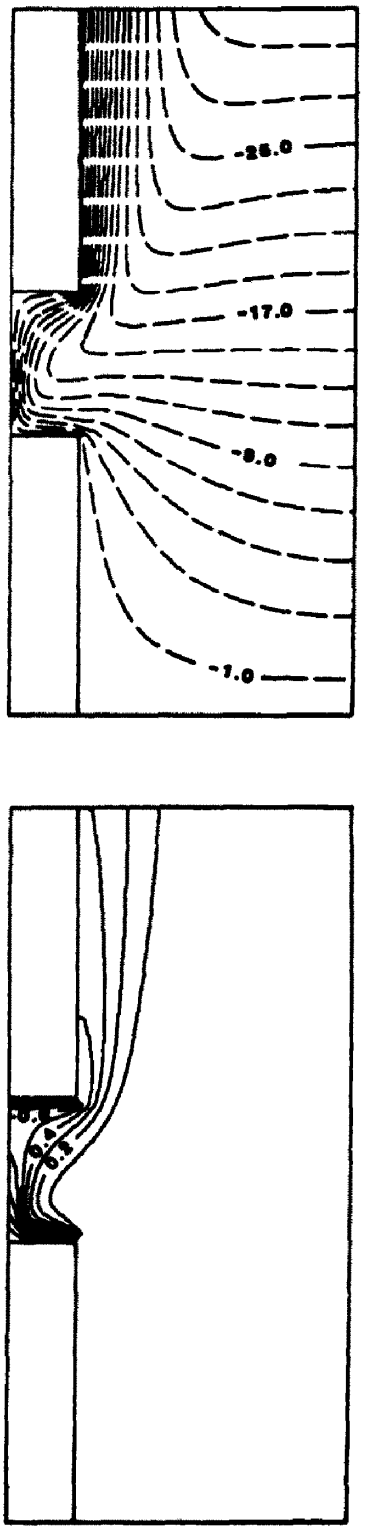

FIG. 12. Streamlines and isotherms for $\theta_2 = 1$, $A = 1$ and $Ra = 100$ at steady state.

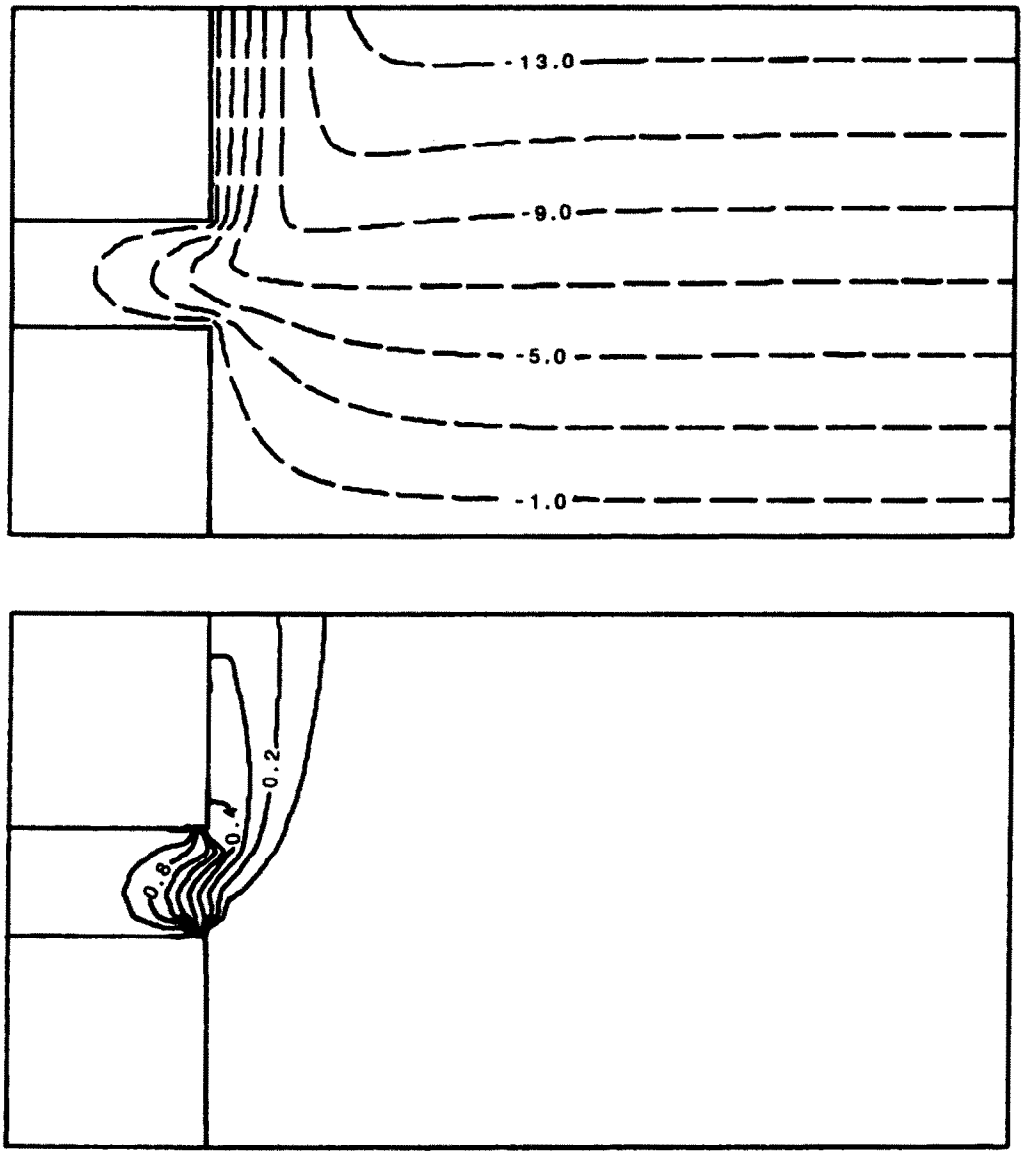

FIG. 13. Streamlines and isotherms for $\theta_2 = 1$, $A = \frac{1}{4}$ and $Ra = 100$ at steady state.

15(a) indicates that, as θ_2 increases, the oscillatory behavior of the cavity Nusselt number becomes more pronounced. Figure 15(b) presents the effect of aspect ratio on the Nusselt number. It can be seen from Fig. 15(b) that decreasing the aspect ratio has a stabilizing effect on the flow fluid.

A summary of the upper block, lower block and cavity Nusselt number is presented in Table 1 for a variety of different conditions. The results show that, in general, the cavity Nusselt number increases with increasing Darcy–Rayleigh number, increasing the upper block temperature and increasing aspect ratio. The influence of different upper block temperature levels on the heat transfer from the lower and upper blocks is complex. As θ_2 increases, the upper block Nusselt number increases considerably due to the larger temperature gradients. At the same time, the lower block Nusselt number increases slightly. This is explained by analyzing the heat transfer from the lower block to the fluid inside the open cavity. The heat transfer from the lower block encounters two opposing effects. The first effect is due to the nature of flow along the lower block, which is more vigorous for higher θ_2 that initially gives rise to higher heat transfer to fluid elements. Secondly, due to higher core temperature for higher θ_2, the capacity of the fluid particles next to the lower block to remove heat from the block is decreased. Consequently, as θ_2 increases, the lower block Nusselt number slightly increases.

4.2. *Comparisons*

In order to check the validity and the accuracy of the numerical scheme used, the computer program was slightly modified through its boundary

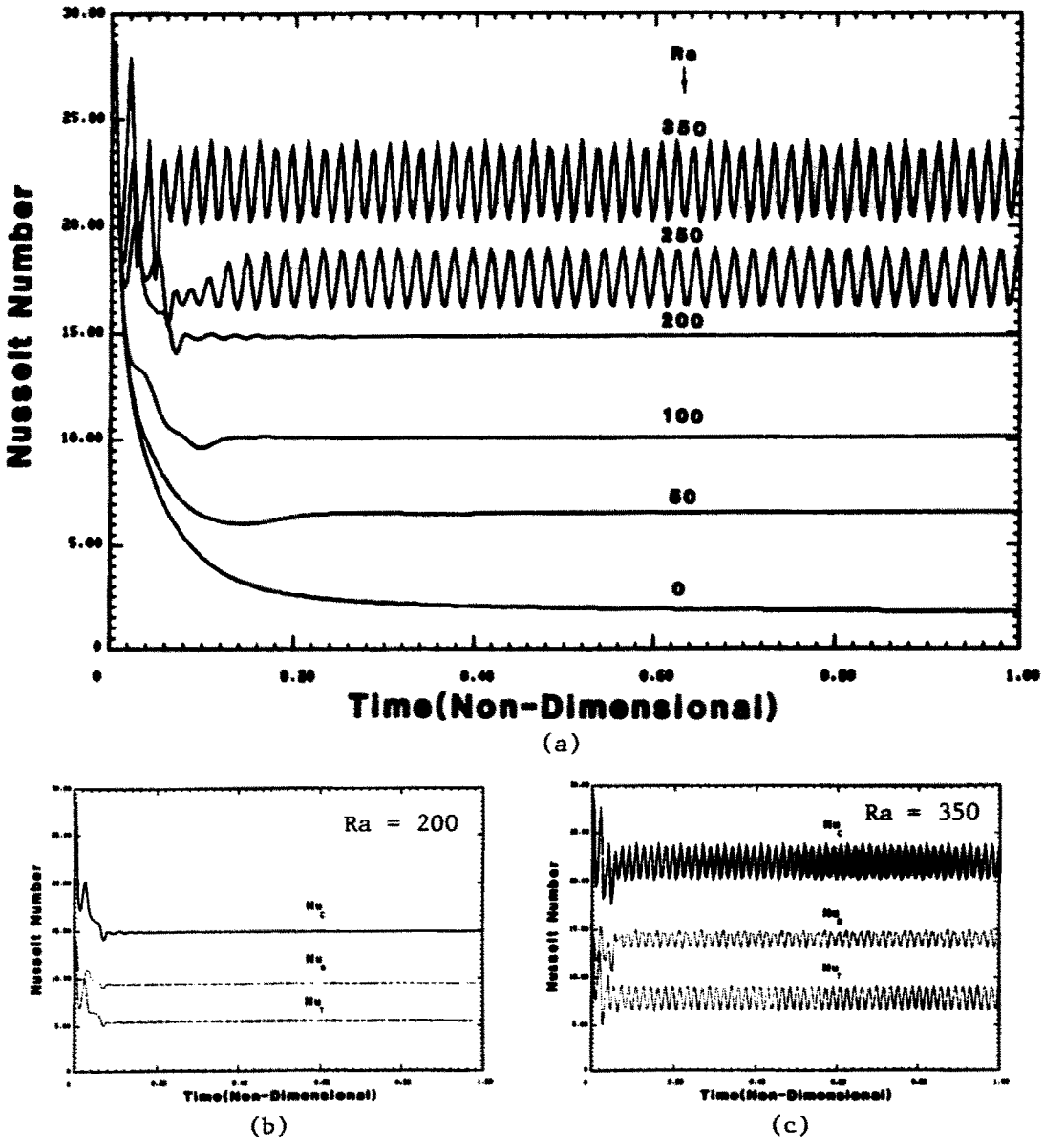

FIG. 14. (a) Time history of the cavity Nusselt number for $\theta_2 = 1$, $A = \frac{1}{2}$ and different Darcy–Rayleigh numbers. (b) Time history of the lower, upper block and cavity Nusselt numbers for $\theta_2 = 1$, $A = \frac{1}{2}$ and $Ra = 200$. (c) Time history of the lower, upper block and cavity Nusselt numbers for $\theta_2 = 1$, $A = \frac{1}{2}$ and $Ra = 350$.

conditions. This modification was done by imposing the adiabatic far field boundary condition at the aperture plane of the open cavity and changing its orientation by 90° in the clockwise direction. The new configuration is the familiar porous medium problem, which is enclosed by rectangular boundaries.

Comparisons were made with the work of Bankvall [5] using the grid sizes of 21×21, aspect ratio of 1, and $Ra \leqslant 200$. The results indicate a deviation of about 14% in the worst case ($Ra = 200$) from that of Bankvall's. Due to the explicit scheme employed in ref. [5], this type of deviation can be expected.

Furthermore, comparisons were also performed with the work of Shiralkar *et al.* [6] for the grid sizes of 81×51, an aspect ratio of 1, and $Ra \leqslant 1000$. As mentioned in ref. [6] beyond a value of $Ra > 1000$, convergence was not possible due to numerical instabilities associated with higher rates of convection. The computed Nusselt numbers from this investigation and the corresponding ones reported in ref. [6] are tabulated in Table 2. As can be seen from Table 2 the agreement is quite good.

5. CONCLUSIONS

Buoyancy-driven flow in an open-ended cavity with obstructing porous medium is investigated in this work. A detailed study of the flow characteristics as

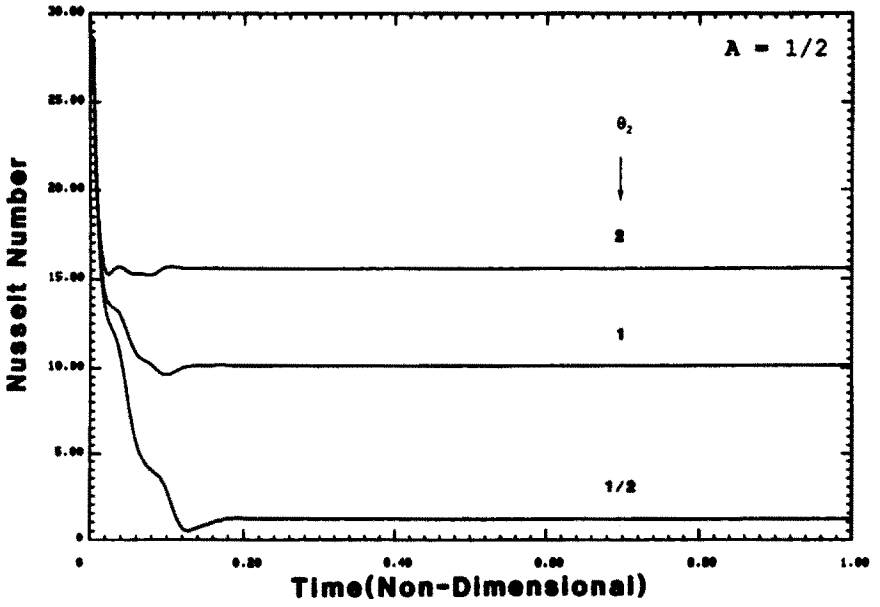

(a)

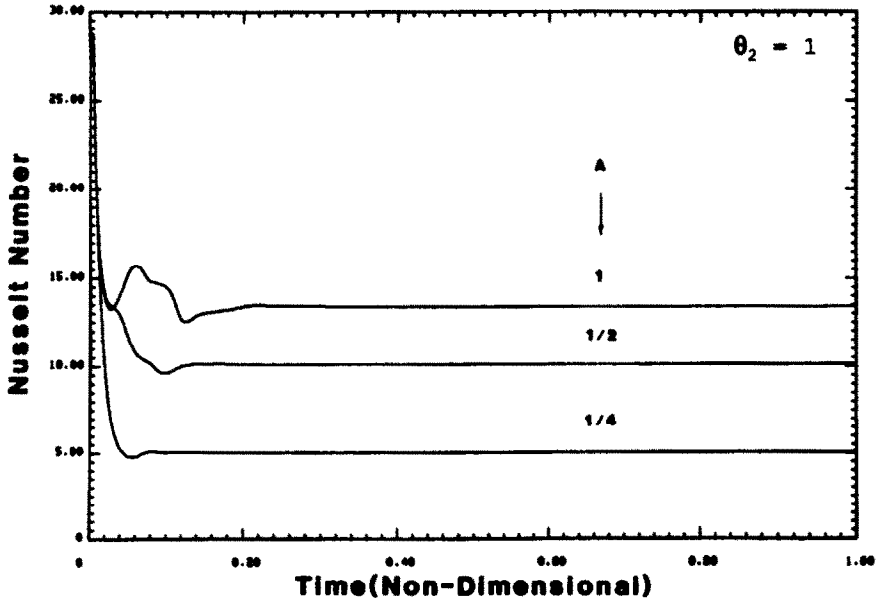

(b)

FIG. 15. (a) Time history of the cavity Nusselt number for $Ra = 100$, $A = \frac{1}{2}$ and different θ_2. (b) Time history of the cavity Nusselt number for $Ra = 100$, $\theta_2 = 1$ and different A.

well as the heat transfer analysis inside the open-ended cavity is performed. Steady state as well as transient results have been obtained through solution of the momentum and energy equations for various Darcy–Rayleigh numbers, aspect ratios and different temperature levels.

The numerical results indicate that the flow field inside the open-ended cavity and in the vicinity of the aperture plane is relatively insensitive to the far field boundary conditions provided that the boundaries are set far enough from the opening. The results also show that the external corners in an open-ended cavity present a crucial influence on the flow pattern and the heat transfer process. Their influence is identified as the vorticity generation and flow instabilities augmentation at the corners. The transient results show that thermal instabilities initially develop along the lower block but disappear at later times as the flow penetrates further into the open cavity. The transient results also indicate that the vorticity is fed into the

Table 1. Summary of the steady-state Nusselt numbers for different cases

Ra	$(A = \frac{1}{2}/\theta_2 = \frac{1}{2}, \theta_2 = 1, \theta_2 = 2)$			$(A = 1/\theta_2 = 1)$	$(A = \frac{1}{4}/\theta_2 = 1)$
10	2.496†				
	1.576‡				
	0.920§				
20	3.664				
	2.445				
	1.219				
50	0.449	6.578	10.831		
	4.271	4.541	4.873		
	−3.822	2.037	5.958		
100	1.183	10.168	15.622	13.412	5.054
	6.742	6.870	7.018	7.543	3.668
	−5.559	3.298	8.604	5.869	1.386
200	2.590	14.884	21.643		
	9.416	9.439	9.463		
	−6.826	5.445	12.180		
250	18.93–16.20				
	11.83–10.78				
	7.10–5.42				
350	23.60–22.28				
	14.41–13.17				
	9.19–7.11				

† The cavity Nusselt number.
‡ The lower block Nusselt number.
§ The upper block Nusselt number.

aperture plane by the lower block eddies, causing the oscillatory behavior in both the lower and upper block heat transfer rates. The results also illustrate that flow unsteadiness arises from values of $Ra \geqslant 250$. The unsteadiness appears as a sequence of recirculating eddies, which originate at the corner of the lower block. These eddies flow along the lower block toward the symmetry line, where they rise. This phenomenon has a periodic effect on the heat transfer inside the open cavity. It is found that decreasing the aspect ratio has a stabilizing effect on flow field. The influence of an increase in the temperature of the upper block is to considerably enhance the heat transfer from the upper block while slightly increasing that of the lower block.

Table 2. Comparison of the Nusselt numbers for various Darcy–Rayleigh numbers

Ra	Nu	Nu^*
100	2.967	3.115
200	4.774	4.976
500	8.938	8.944
700	11.125	10.969
1000	14.140	12.534

The asterisk (*) indicates the values from ref. [6].

REFERENCES

1. S. Ostrach, Natural convection in enclosures, *Adv. Heat Transfer* **8**, 161–227 (1972).
2. P. Cheng, Heat transfer in geothermal systems, *Adv. Heat Transfer* **14**, 1–105 (1979).
3. S. Ostrach, Natural convection heat transfer in cavities and cells, Keynote paper at the Seventh International Heat Transfer Conference, Munich (1982).
4. B. K. C. Chan, C. M. Ivey and J. M. Barry, Natural convection in enclosed porous media with rectangular boundaries, *J. Heat Transfer* **92**, 21–27 (1970).
5. C. G. Bankvall, Natural convection in vertical permeable space, *Wärme- und Stoffübertr.* **7**, 22–30 (1974).
6. G. S. Shiralkar, M. Haajizadeh and C. L. Tien, Numerical study of high Rayleigh number convection in a vertical porous enclosure, *Numer. Heat Transfer* **6**, 223–234 (1983).
7. P. Le Quere, J. A. C. Humphrey and F. S. Sherman, Numerical calculation of thermally driven two-dimensional unsteady laminar flow in cavities of rectangular cross section, *Numer. Heat Transfer* **4**, 249–283 (1981).
8. F. Penot, Numerical calculation of two-dimensional natural convection in isothermal open cavities, *Numer. Heat Transfer* **5**, 421–437 (1982).
9. Y. L. Chan and C. L. Tien, Laminar natural convection in shallow open cavities, 21st ASME–AIChE National Heat Transfer Conference, Natural Convection in Enclosures, Vol. 26, pp. 77–82 (1983).
10. K. Vafai and C. L. Tien, Boundary and inertia effects on convective heat transfer in porous media, *Int. J. Heat Mass Transfer* **25**, 1183–1190 (1982).
11. P. J. Roache, *Computational Fluid Dynamics*. Hermosa, Albuquerque (1976).
12. A. Bejan, *Convection Heat Transfer*. Wiley, New York (1984).

CONVECTION NATURELLE DANS DES CAVITES OUVERTES AVEC UN MILIEU POREUX OBSTRUANT

Résumé—La convection naturelle dans une cavité à extrémité ouverte avec un milieu obstacle tel qu'un matériau poreux est analysé dans ce travail. Les résultats numériques de l'écoulement relatifs aux champs de vitesse et de température sont donnés pour le domaine de nombre de Darcy–Rayleigh $Ra \leqslant 350$. On discute l'importance des coins externes dans la génération de tourbillon et d'augmentation d'instabilité d'écoulement. On étudie la présence de "bosses" et le comportement périodique dans la variation du nombre de Nusselt avec le temps. Les effets des variables importantes comme le rapport de forme, la différence de température et le nombre de Darcy–Rayleigh sur le champ de vitesse et sur le nombre de Nusselt de la cavité sont analysés. Des comparaisons sont aussi faites avec des études antérieures de convection naturelle dans une cavité remplie par un milieu poreux.

NATÜRLICHE KONVEKTION IN OFFENEN, MIT EINEM PORÖSEN MEDIUM GEFÜLLTEN HOHLRÄUMEN

Zusammenfassung—In dieser Arbeit wird die natürliche Konvektion in einem offenen, mit einem porösen Medium gefüllten Hohlraum untersucht. Es werden numerische Ergebnisse für Strömungs- und Temperaturfelder bei Darcy–Rayleigh-Zahlen $Ra \leqslant 350$ angegeben. Die Bedeutung von äußeren Ecken bei der Wirbelbildung und bei der Vergrößerung der Strömungsinstabilität wird diskutiert. Der Einfluß von 'Höckern' und das periodische Verhalten bei der zeitlichen Änderung der Nusselt-Zahl werden untersucht. Es werden die Einflüsse wichtiger Parameter wie das Seitenverhältnis, die Temperaturdifferenz und die Darcy–Rayleigh-Zahl auf das Strömungsfeld und die Nusselt-Zahl im Hohlraum untersucht. Vergleiche mit früher veröffentlichten Studien über die natürliche Konvektion in einem Hohlraum, der mit einem porösen Medium gefüllt ist, werden angestellt.

ЕСТЕСТВЕННАЯ КОНВЕКЦИЯ В ОТКРЫТЫХ ПОЛОСТЯХ, ЗАПОЛНЕННЫХ ПОРИСТОЙ СРЕДОЙ, ПРЕПЯТСТВУЮЩЕЙ ТЕЧЕНИЮ

Аннотация—Анализируется вызываемая подъемной силой конвекция в открытой полости, заполненной пористым материалом, который препятствует течению. Приведены численные результаты для полей течения и температуры при значениях числа Дарси–Рэлея $Ra \leq 350$. Обсуждается роль внутренних углов полости в генерировании завихренности и усилении неустойчивости течения. Исследуются появление "горбов" на кривых и периодические изменения во времени числа Нуссельта. Изучается влияние таких важных переменных, как отношение размеров полости, разность температур и число Дарси–Рэлея, на поле течения и число Нуссельта для полости. Проведено сравнение с известными результатами по исследованию естественной конвекции в полости, заполненной пористым материалом.